# Methanol tolerant $Pt_2CrCo$ catalysts supported on ordered mesoporous carbon for the cathode of DMFC (Code A2_99)

L.M. Rivera Gavidia[1], G. García[1*], V. Celorrio[2, a], M.J Lázaro[2], E. Pastor [1*]

[1]*Instituto de Materiales y Nanotecnología, Universidad de La Laguna, Avda. Astrofísico Francisco Sánchez s/n, 38071 La Laguna, Santa Cruz de Tenerife, Spain*

[2] *Instituto de carboquímica (CSIC) Miguel Luesma Castan 4, 50018 Zaragoza, Spain*

* Corresponding author. Tel.: +34 922 318071; fax: +34 922 318002

E-mail address: ggarcia@ull.edu.es (Gonzalo García).

E-mail address: epastor@ull.edu.es (Elena Pastor).

[a]Present Address: School of Chemistry, University of Bristol, Cantocks Close, Bristol BS8 1TS, United Kingdom

**Abstract**

Graphitized ordered mesoporous carbon CMK-3-R8 supported $Pt_2CrCo$ electrocatalysts were synthetized by the borohydride reduction method (BM) and then submitted to a reductive thermal treatment (TT) at 300, 500 and 700 ºC with the aim to improve their catalytic activity toward the oxygen reduction reaction (ORR) and the methanol tolerance. Atomic composition and total metal loading were determined by energy dispersive X-ray (EDX) analysis and the values obtained were close to the nominal ones, i.e. 20 wt.% $Pt_2CrCO$/CMK-3. Electrochemical measurements were carried out using rotating disk electrode (RDE) technique in oxygen-saturated sulphuric acid solution in absence and presence of dissolved methanol. Besides other species and parameters, X-ray diffraction (XRD) and X-ray photoelectron spectroscopy (XPS) analysis revealed the formation of an ordered $Pt_3Cr$ alloy phase and the surface enrichment by $Cr_2O_3$ species with the rise of the annealing temperature. The last, in conjunction with the absence of Pt sites with (110) orientation, enhances the catalytic activity toward the ORR and the methanol tolerance. Kinetic parameters are reported and analyzed in terms of the physicochemical properties of the catalysts obtained by the X-ray techniques.

***Keywords****: ORR, DMFC, methanol tolerance, thermal treatment, PtCrCo alloys, graphitized ordered mesoporous carbon.*

## 1. Introduction

Fuel cells (FCs) are promising electrochemical energy converters for a diversity of applications. They have the potential to provide environmentally friendly energy conversion at high efficiency and power density. Proton exchange membrane fuel cell (PEMFC) and direct methanol fuel cell (DMFC) work at low temperatures and are expected to succeed for applications with low-medium power densities such as mobile phones, laptops and cars [1]. DMFC offers several advantages in comparison to PEMFC. Some of them are the facile liquid-feed system, in which fuel-processing equipment is not required, the easy humidification and heat management modules since liquid-methanol can provide the necessary humidification and heat control and transport [2].

One of the main research areas in PEMFC and DMFC involves the oxygen reduction reaction (ORR) at the cathode of the FC. The great importance of this issue is related to the slow ORR kinetics that is responsible for more than half of the overall cell voltage loss during FC working operation. In this context, DMFC has several drawbacks in comparison to PEMFC, especially the crossover of methanol from the anode to the Pt-based cathode that limits the overall performance [1-3]. The last produces a mixed potential at this electrode, that is, the ORR and the methanol oxidation reaction occurring simultaneously, and consequently the cell voltage falls.

To overcome this issue, methanol tolerant catalysts are needed and it is common to study the catalytic activity of platinum alloys with transition metals for the ORR in the presence of methanol [3]. In addition, the catalysts support was found to play an important role for both reactions and therefore several studies were devoted to analyze its effect [3-5]. Thus, a variety of bi/trimetallic platinum-based catalysts supported on diverse materials have been used to increase the methanol tolerance and the ORR activity. These improvements have been ascribed to different factors such as the surface area, changes in the Pt–Pt interatomic distance and the Pt electronic configuration, as well as, to the third body effect [5].

In this sense, ordered mesoporous carbons (OMC) and particularly CMK-3 carbons present several advantages when are used as carbon supports for fuel cell catalysts [6], for instance: i) low cost of fabrication because SBA-15 template is inexpensive and easy to synthetize; ii) easy diffusion and mass transportation control though the mesoporous structure; and iii) promotion high and homogeneous metal dispersion. CMK-3 carbon

materials present an accessible surface area on the range of 200-1000 $m^2$ $g^{-1}$ depending on the synthetic method, which can be several orders of magnitude higher than other mesoporous supports such as the commercially available Vulcan XC-72R (200 $m^2$ $g^{-1}$) [7], carbon nanofibers (95 $m^2$ $g^{-1}$) [8], or carbon nanocoils (120 $m^2$ $g^{-1}$) [9]. Furthermore, our group has previously shown that heat-treated CMK-3 carbon materials present high corrosion resistance and elevated activity, when they are used as catalytic supports [10].

Different Pt-based catalysts supported on OMC were reported in the bibliography [6,11], and in most cases, showed an enhanced catalytic activity toward the ORR and methanol oxidation in comparison with commercial catalysts. Accordingly, Ding et al. reported a Pt/CMK-3 electrocatalyst with low Pt content (~10 wt. %) that showed higher ORR activity than Pt commercial catalyst, even though the Pt/CMK-3 particle size was larger. They proposed that the activity rise was due to the combination of several factors: metal particle size, surface area, pore ordering and pore diameter [12]. For DMFC cathode side, Choi et al. designed a novel catalysts using OMC, which consisted of Pt clusters inside the mesoporous structure. The MEA prepared with this material presented 40-60 mV open circuit voltage higher than Pt-ETEK catalysts in a DMFC. The authors suggested that the presence of micropores and the Pt location inside the structure delay the methanol diffusion and conversely promotes the oxygen access [13]. Finally, Liu et al. established high CO tolerance for Pt/OMC (~15 wt. % of Pt loading) when the Pt nanoparticles are placed inside tube-type OMC structures [14].

On the other hand, it has been reported that carbon supported PtCr, PtCo and PtNi catalysts develop higher performances for the oxygen reduction reaction in comparison to Pt/C [15]. Shuo Chen et al. described a four-fold improvement toward the ORR by PtCo/C alloy nanoparticles [16]. Furthermore, PtCo nanoparticles synthetized by water-in-oil microemulsion method followed by a thermal treatment at 875 ºC under a reductive atmosphere showed higher catalytic activity toward ORR than commercial Pt/C catalyst [17]. This improvement was confirmed by Baglio et al. observing an increment of the DMFC performance using a PtCo alloy as cathodic material [18]. Additionally, high methanol tolerance during the ORR at PtCo materials in acidic media was reported [19-22]. It was also reported that Cr and Co elements increase the active surface for bi-metallic (PtCr and PtCo) and tri-metallic (PtCrCo) alloys after being annealed at 900 ºC due to Pt surface segregation [19].

In the current study, mesoporous carbon supported $Pt_2CrCo$ ($Pt_2CrCo$/CMK-3) catalyst was synthesized and subjected to different thermal treatments. Then, the materials were

characterized by several physicochemical (X-ray diffraction (XRD), X-ray photoelectron spectroscopy (XPS) and energy dispersive X-ray spectroscopy (EDS)) and electrochemical (rotating disk electrode (RDE), lineal sweep voltammetry (LSV) and cyclic voltammetry (CV)) techniques in pure and methanol-containing electrolytes.

## 2. Experimental

### *2.1. Catalyst synthesis*

CMK-3 mesoporous carbon was synthesized according to previous works [23, 24] to be used as carbon supporting material. Briefly, ordered mesoporous carbons (CMK-3-R8) were prepared by incipient wetness impregnation of SBA-15 silica with furan resin (Huttenes-Albertus) as carbon precursor. The silica material SBA-15/R8 contained a mass ratio of TEOS/P123 equal to 8 (R8). Subsequently, the impregnated silica was carbonized at 700 °C for 2 h. The obtained silica-carbon composite was washed with a 5 M NaOH (Panrec) solution for 12 h at 60 ºC to remove the silica particles and washed with distilled water. [9, 24, 25]. Then, it was dried at 108 ºC for 24h. The carbon material obtained was subjected to a thermal treatment at 1500 ºC in a graphite electrical furnace for 1 h under argon flow, using a heating rate of 10 ºC $min^{-1}$. The textural properties of the carbon support are reported in Table 1. CMK-3-R8 presents a high specific surface area of 273$m^2.g^{-1}$. In the rest of this work, the graphitized carbon material will be referred as CMK-3.

Appropriate amounts of metal precursors ($H_2PtCl_6$, $CrCl_3$ and $CoCl_2$, Sigma-Aldrich) were employed to obtain PtCrCo catalyst with atomic ratio (2:1:1) and nominal metal loading of 20 wt. % on CMK-3.

The borohydride method (BM) was applied to reduce the metal precursors. Briefly, an aqueous suspension of the mesoporous carbon was obtained by stirring during ca. 24 h. After that, a water solution containing the metal precursors was slowly added to the carbon suspension and then the pH was adjusted to 5 with a NaOH solution. Next, metal ions were reduced by the gradual addition a sodium borohydride (99%, Sigma Aldrich) solution under sonication at a constant temperature of 20 °C. Subsequently, catalysts were filtered and copiously washed with ultrapure water. Finally, the material was submitted to a thermal treatment during 2 h under a reductive atmosphere ($N_2$:$H_2$ ratio of 95:5; 10 $mLmin^{-1}$) at different temperatures. On the basis of the true composition and the thermal treatment used, the electrocatalysts are denoted as: 1) $Pt_2CrCo$/CMK-3-

WTT without thermal treatment and 2) $Pt_2CrCo$/CMK-3-T where T is the temperature for thermal treatment (300, 500 and 700 ºC).

*2.2. Physicochemical characterization*

Catalysts were characterized by X-ray diffractograms (XRD) using a PANalytical X'Pert Pro X-ray diffractometer operating with Cu Kα radiation (λ = 0.15406 nm) generated at 40 kV and 20 mA. Scans were done at 0.04º $s^{-1}$ for 2θ values between 20º and 100º. To avoid the influence of peak overlapping of a broad band of the amorphous carbon and other reflections, the (220) peak reflection of face centered cubic (*fcc*) structure of Pt was used to estimate the crystallite size by the Debye-Scherrer equation [26]. The Pt-Pt interplanar spacing was determined from the lattice parameters that were obtained by refining the unit cell dimensions by the least squares method [27].

The atomic composition and total metal loading of the electrocatalysts was determined by energy dispersive X-ray analysis (EDX) coupled to the scanning electron microscope Jeol JSM 6300 with a silicon doped with lithium 6699 ATW detector applying 20 keV.

X-ray photoelectron spectroscopy (XPS) analysis was performed with a Thermo-Scientific equipment operating with Al Kα line radiation (1486.6 eV), containing a twin crystal monochromator and yielding a focused X-ray spot with a diameter of 400 microns at 3 mA × 12 kV. Charge compensation was achieved with the flood gun system that provides low energy electrons and argon ions from a single source. The samples were placed into a pre-chamber during 4–5 h. The analysis chamber pressure during the measurement was maintained below $5 \times 10^{-8}$ mbars.

The binding energies (BE) were calibrated using the C 1s peak at 284.6 eV to take into account charge effects. The peaks areas were calculated by fitting the experimental spectra using gaussian/lorentzian combined shapes, after the elimination of background noise upon use of Shirley-type curves. The surface atomic contents for each component were calculated from such fittings, employing the corresponding atomic sensitivity factors. The XPS data interpretation was carried out using standard data from Perkin-Elmer Corporation X-ray photoelectron spectroscopy handbook [28]. Deconvolution of the XPS spectra were carried out by the XPSPEAK 41 software.

A JEOL-2000 FXII microscope operating at an accelerating voltage of 200 kV was used to obtain transmission electronic microscope (TEM) images, which were utilized to

evaluate the morphology of the catalysts. The average particle diameter of each catalyst was calculated measuring the diameter of at least 300 metallic particles.

### *2.3. Electrochemical characterization*

The electrochemical measurements were carried out in a three-electrode half-cell at room temperature (25 ºC) controlled by an Autolab PGSTAT302N potentiostat-galvanostat. A carbon rod was used as a counter electrode, while the reference electrode was a reversible hydrogen electrode (RHE) in the supporting electrolyte (0.5 M $H_2SO_4$, Merck p.a.). Potential values were referred to this electrode. The working electrode was a rotating electrode (RDE) containing a glassy carbon disk (geometrical area = 0.071 $cm^2$) where a catalyst ink was deposited. The ink containing in the catalyst was prepared under sonication by mixing 2 mg catalyst, 15 µL Nafion® (5%, Sigma-Aldrich) and 500 µL water (Milli-Q, Millipore). Then, an aliquot (20 µL) of the ink was carefully dried onto the glassy carbon disk under Ar atmosphere. Electrolyte solution occasionally was deoxygenated with Ar (Air Liquide 99.999%), saturated with $O_2$ (Air Liquide 99.995%) to perform the measurements related to the ORR or with CO (99.997%, Air Liquide) for CO-stripping experiments. Methanol (Merck p.a.) was used for the ORR study in presence of alcohol. Both, electrolyte and methanol solution were prepared using high purity water provided by MilliQ - Millipore system (18.2 MΩ $cm^{-1}$ of resistivity).

Prior to each study, an activation step of the working electrode was performed, which consists of potentiodynamic cycles between 0.10 and 0.70 V at 0.20 V $s^{-1}$ until a reproducible voltammogram was achieved. Then, a blank cyclic voltammogram (BCV) was recorded at 0.02 V $s^{-1}$ between 0.05 and 0.9 V. $O_2$ was bubbled during 20 min before each ORR experiment and an oxygen atmosphere was maintained during all measurements. Steady state polarization curves were carried out between 1.00 and 0.20 V at rotating speeds of 400, 600, 900, 1600 and 2500 rpm to evaluate the ORR kinetics parameters. In this study, the working electrode was introduced into the electrolyte at a controlled potential of 1 V, and subsequently, a linear sweep voltammetry (LSV) curve was initiated in the negative going direction at scan rate of 0.002 V $s^{-1}$. The voltammetric profiles of the catalyst and the ORR experiments were studied in absence and presence of methanol in solution. With this end, 0.5, 1, 2 and 3 M methanol solutions in 0.5 M sulphuric acid medium were employed. CO stripping experiments were recorded at 0.02 V $s^{-1}$ after bubbling CO through the cell for 10 min while keeping

the electrode at 0.07 V, followed by $N_2$ purging to completely remove the excess of CO [29]. The electroactive surface area (ESA) was obtained from CO stripping experiments.

## 3. Results and discussion

### *3.1. Physicochemical characterization of $Pt_2CrCo$/CMK-3 catalysts*

The metal loading and metal composition of synthesized materials were determined by EDX analysis. Values close to the nominal one were obtained for all catalysts and are summarized in Table 2. X-ray diffractograms are depicted in Figure 1, in which the typical (111), (200), (220), (311) and (222) diffraction patterns of the face-centered cubic (*fcc*) structure of platinum are discerned [15,17]. It is noteworthy that the five diffraction peaks of platinum are to some extent shifted to higher angles (see Table 2) in comparison to carbon-supported platinum catalyst (lattice parameter = 0.3915 nm [30]), which indicate a lattice contraction and alloy formation. Interestingly, the lattice parameter and the Pt-Pt interplanar distance of the $Pt_2CrCo$/CMK-3 materials follow a volcano-shaped curve with the rise of the thermal procedure (Figure 2). This result may be occasioned by the surface reconstruction of the nanoparticles that results in a deviation from the lattice parameter mean value due to the surface to nanocrystal core ratio is large or by internal modification of the involved species [25], which in turn may alter the the electronic properties of the d-band of Pt [31].

In addition to the five main characteristic features of the Pt *fcc* structure, a small but visible diffraction peak is developed at ca. 36º, which is related to crystalline $Cr_2O_3$ species (Figure 1b) [15]. The intensity of the last signal slightly increases with the rise of the heating procedure. Also, $Pt_2CrCo$/CMK-3-700 electrocatalyst develops three weak diffraction patterns at 23º, 33º and 53º, which are associated to the superlattice planes of an ordered $Pt_3Cr$ alloy phase (Figure 1a,b) [30]. Peaks related to Pt and Co oxides phases were not observed for catalysts thermally treated up to 700 ºC, although amorphous metallic oxides cannot be discarded [19].

Diffraction peaks for $Pt_2CrCo$/CMK-3 catalysts in Figure 1 are sharper with the rise of the heating procedure indicating an increment of the metal particle size [32]. Average metal crystallite size was calculated using the Scherrer' equation [33, 34] and, as expected, the values exponentially grow from 4.7 to 13.5 nm with the increase of the temperature of the thermal treatment (Figure 2). Thus, the annealing procedure provokes important morphologic and structural changes in the metallic materials, in

agreement with previous works [17, 32]. Remarkable are the crystallite growth of the $Pt_2CrCo$/CMK-3-700 material and the lack of relationship between particle size and lattice parameter. Table 2 summarizes the above mentioned parameters.

The rise of the particle size and the high stability of the catalyst support with the increment of the thermal procedure were proved by TEM (see *Supporting Information*). TEM images show that metal deposition is uniform and highly dispersed, as well as, it does not block the mesoporous structure of the catalyst support and therefore the primary pore size is not compromised.

XPS was used to provide essential information on the oxidation state of the elements in the materials and the stoichiometry at the catalyst surface. XPS spectra corresponding to the Pt 4f orbital are reported in Figure $3a_{1-4}$. The Pt 4f signal was deconvoluted into two distinguishable doublets of different intensity. For the Pt $4f_{7/2}$ transition, the components at 71.3-71.8 and 72.6-73.3 eV are attributed to $Pt^0$ and $Pt^{2+}$ ($Pt(OH)_2$ and PtO species), respectively [28]. Interestingly, no contribution of $PtO_2$ was discerned and the binding energies for $Pt^0$ and $Pt^{2+}$ are slightly shifted toward more positive values in comparison to bare Pt in carbon-supported Pt material [35]. The Cr 2p spectrum consists of two signals related to the $2p_{3/2}$ and $2p_{1/2}$ transitions (Figure $3b_{1-4}$) [28]. The Cr 2p signal was deconvoluted into three distinguishable doublets of different intensity. For the Cr $2p_{3/2}$ transition, the components at 575.8-576.2, 576.4-577.5 and 577.8-578.9 e.V are attributed to $Cr(OH)_3$ ($Cr^{3+}$), $Cr_2O_3$ ($Cr^{3+}$) and $CrO_3$ ($Cr^{6+}$), respectively [28,36]. Remarkable is the absence of metallic chrome at the surface of the catalysts. Figure $3c_{1-4}$ shows the Co 2p core level orbitals, in which the transitions of the Co $2p_{3/2}$ (~781 eV) and Co $2p_{1/2}$ (~796 eV) and their corresponding satellites are discerned [28,36]. Since the full Co 2p signal is challenging, only the Co $2p_{3/2}$ transition signal was deconvoluted into three singlet peaks of different intensity [36]. In this way, the components at 777.7-778.5, 780.7-781.3 and 784.3-785.1 e.V are attributed to $Co^0$, CoO ($Co^{2+}$) and $Co_2O_3$ ($Co^{3+}$), respectively.

XPS peak positions and contribution in % for the different components of each element are reported in table 3 and depicted in Figure 4 for the different thermal treatments. The top panel of the Figure 4 clearly shows the segregation of chromium to the catalyst surface applying the thermal procedure at 700 ºC. Meanwhile, the surface concentration of platinum increases at $Pt_2CrCo$/CMK-3-300 and $Pt_2CrCo$/CMK-3-500 materials and then decreases at $Pt_2CrCo$/CMK-3-700. In this context, it is evident the close correlation between Pt surface concentration and the ESA that is connected to the amount of active

Pt sites onto the catalyst surface (see below). Also, it is noticeable that the Pt surface concentration is not linked with the crystallite size at least for those materials annealed at temperatures ≤ 500 ºC (Figure 2). Co surface concentration is quite similar for $Pt_2CrCo$/CMK-3-WTT, $Pt_2CrCo$/CMK-3-300 and $Pt_2CrCo$/CMK-3-500, but it drops when thermal procedure at 700 ºC was applied. Bottom panel of Figure 4 depicts the contribution for the different oxidation states of the elements involved at the catalyst surface. Most important features involve: i) the strong increment and decrease of $Cr^{+3}$ and $Cr^{+6}$ species, respectively, with the rise of the annealing temperature; ii) the inflection point for Pt species at the $Pt_2CrCo$/CMK-3-300 material, in which $Pt^0$ and $Pt^{+2}$ slightly decreases and increases, respectively, in comparison to $Pt_2CrCo$/CMK-3-WTT; iii) the material treated at 300 ºC presents the closest surface concentration of $Cr^{+3}$ and $Cr^{+6}$ species; iv) moderate increment and fall of $Pt^0$ and $Pt^{+2}$ species, respectively, with increasing the treatment temperature ≥ 500 ºC; and v) $Co^{+2}$ and $Co^{+3}$ species decreases and increases monotonically with rising the annealing temperature, which suggests an increment of charge transfer from cobalt toward the other species.

### *3.2. Electrochemical studies*

Figure 5 shows the blank cyclic voltammograms (CVs) for all synthesized catalysts in the supporting electrolyte. Currents are normalized by the ESA, which was obtained from CO stripping experiments (Figure 6). It can be observed that $Pt_2CrCo$/CMK-3 catalysts reveal the typical profile of carbon supported Pt electrodes, i.e., hydrogen adsorption/desorption features are clearly observed at E < 0.4 V [37]. Nevertheless, some specific outcomes can be discerned such as the high capacitive current that must be associated to the mesoporous structure of the catalyst support material (CMK-3) and the decrease of the reversible peaks at ca. 0.125 V associated to hydrogen adsorption/desorption on Pt sites with (110) orientation with annealing temperatures higher than 500 ºC [11,38]. The last is clearly evident at the $Pt_2CrCo$/CMK-3-700 catalyst.

CO stripping experiments were used to study the CO tolerance and to obtain the electroactive surface area (ESA) that is used for current normalization. ESA were determined from the integration of the current involved in the oxidation of a CO monolayer taking into account that CO adsorbs only on Pt and assuming a charge of 420 ??C $cm^{-2}$ [39]. The ESA normalized by the amount of Pt into the working electrode

(EASA) was also calculated and included in the Table 4. Noteworthy is that both (ESA and EASA) parameters are associated to the amount of Pt in the catalyst. Indeed, the ESA follows the same profile to that developed for the surface concentration of Pt (see Figure 4). In addition, the EASA values acquired are in agreement to those reported in the bibliography using ordered mesoporous carbon (OMC) as catalyst support [32, 35].

The CO stripping voltammograms recorded for the different catalysts are shown in Figure 6, together with the subsequent voltammograms. It is observed that CO is completely removed after the first CV. Also, similar voltammetric profiles of both blank (Fig. 5) and second voltammogram after CO stripping are achieved. The last indicates an electrochemical stability of the catalysts under study in the potential range applied for these studies. All catalysts develop an onset potential for the CO oxidation reaction close to 0.35 V followed by a broad anodic current and anodic peak/s. The broad anodic feature developed in the voltammograms is associated to surface sites with different catalytic activity toward the CO oxidation reaction [40]. In addition, $Pt_2CrCo$/CMK-3-WTT develops two anodic peaks at ca. 0.72 and 0.83 V associated to two surface sites with different activity. $Pt_2CrCo$/CMK-3-300 also develops two main anodic peaks, but shifted to lower potentials (0.71 and 0.79 V) than the catalyst without the thermal treatment. On the other hand, $Pt_2CrCo$/CMK-3-500 and $Pt_2CrCo$/CMK-3-700 develop only one main anodic peak centered at ca. 0.76 and 0.75 V, respectively. Noticeable is the shift toward more negative potentials of the main CO oxidation peaks and increment of the charge under broad anodic current developed at lower potentials than 0.6 V with the rise of the annealing procedure. The last indicates an enhancement of the CO tolerance with stronger heating treatment [32], which may be ascribed to the surface segregation of $Cr_2O_3$ that provides oxygenated species, the formation of an ordered and active $Pt_3Cr$ alloy phase and the surface reconstruction with the concomitant production of active catalytic sites [38,40]. Therefore, the CO tolerance increases in the following order: $Pt_2CrCo$/CMK-3-WTT < $Pt_2CrCo$/CMK-3-300 < $Pt_2CrCo$/CMK-3-500 < $Pt_2CrCo$/CMK-3-700.

The catalytic activity toward the ORR was studied in supporting electrolyte and in methanol-containing solution. Figure 7 shows the polarization curves for all mesoporous carbon supported $Pt_2CrCo$/CMK-3 catalysts recorded in oxygen saturated acid solution at 1600 rpm and 0.002 V $s^{-1}$. All materials develop similar profiles during the ORR but as a general trend, it can be established that the catalytic activity toward this reaction enhances with the thermal treatment. A close inspection of the polarization

curves reveals two well-defined potential ranges: at higher potentials than 0.6 V, in which the process is controlled by kinetic and diffusion; and at lower potentials than 0.6 V, in which the diffusion controls the overall reaction [30, 41]. The top panel of Figure 7 shows that the current density at the region of diffusional control increases with the rise of temperature during the thermal treatment. The activity is also enhanced at the region of mixed control for catalysts treated up to 500 ºC but then decreases for the catalyst annealed at 700 ºC. The bottom panel of Figure 7 depicts the same ORR signals but normalized by the ESA, showing that the PtCrCo/CMK-3-700 catalyst develops the highest activity toward the ORR. The best performance developed by this material may be ascribed to the conjunctions of several factors that bring a suitable catalytic surface, such as the high crystallite size, the lowest Pt-Pt bond distance, the superlattice planes of an ordered $Pt_3Cr$ alloy phase and the high degree of metallic Pt utilization with specific crystalline surface sites (high density of Pt sites with (100) and (111) orientations). In this context, there is a consensus that Pt(100) and Pt(111) sites are more active toward the ORR than Pt sites with (110) orientation [1].

ORR polarization curves at 1600 rpm recorded in 0.5 M and 3 M methanol solution at 0.002 V $s^{-1}$ are given in Figure 8a and 8b, respectively. It is clear an increment of the anodic current related to the alcohol oxidation reaction (mixed potential region) at potentials more positive than 0.6 V for all catalysts, which decreases the overall activity toward the ORR. Nevertheless, an important effect of the temperature of the thermal treatment can be discerned. Indeed, an increment of the methanol tolerance in the region controlled by diffusion is achieved with the rise of the temperature during the heating procedure. The lower methanol activity on $Pt_2CrCo$/CMK-3-700 compared to the other catalysts can be explained on the basis of the ‘‘ensemble effect.’’ Actually, it is well established that for methanol oxidation at least three adjacent Pt sites in the proper spatial arrangement are necessary to activate the deprotonation and chemisorption of methanol. For the $Pt_2CrCo$/CMK-3-700 alloy, according to XPS analysis, the probability of finding three neighboring Pt atoms on the surface is lower than in the other catalysts. Since the dissociative chemisorption of methanol requires several adjacent Pt ensembles, the presence of methanol-tolerant Cr and Co around Pt active sites could hinder methanol adsorption on Pt sites due to the dilution effect. On the other hand, oxygen adsorption, which usually can be regarded as dissociative chemisorption and requires only two adjacent Pt sites, is not influenced by the presence of Cr and Co atoms (or at least is influenced in a less extent).

In order to evaluate the kinetic response of the catalysts toward the ORR in absence of dissolved methanol, the Koutecky- Levich equation was employed [33]:

$$j^{-1} = j_k^{-1} + (0.62nFAD^{2/3}C_0\nu^{1/6}w^{1/2})^{-1} \quad (2)$$

where $n$ is the number of electrons transferred, $F$ is the Faraday constant (96500 C), $A$ is the geometric area of the electrode, $D$ is the diffusion coefficient ($1.4x10^{-5}$ $cm^2s^{-1}$) , $C_0$ is the bulk $O_2$ concentration ($1.1x10^{-6}$ $mol.cm^{-3}$), $\nu$ is the viscosity of the electrolyte (0.010 $cm^2\,s^{-1}$) and $w$ is the angular velocity [33].

Figure 9 shows the Koutecky-Levich plots at two potentials and several disk rotation speeds for the materials prepared in the present paper and Table 4 reports the main results. The electron transferred ($n$) was estimated using the slope obtained from the plot of $j^{-1}vs\ \omega^{-1}$, in which the parallel lines recorded at 0.8 and 0.75 V suggest that the ORR follows a first order kinetics in this potential range [42]. The $n$ value indicates that the 4 $e^-$ route (complete way of reduction of $O_2$ to water) is the governing mechanism for all the catalysts, although an increment in the conversion efficiency of $O_2$ to water is observed with the rise of the thermal treatment that must be related to several factors as described above (see discussion of Figure 5). On the other hand, the $Pt_2CrCo$/CMK-3-500 catalyst develops the maximum kinetic currents in absence of alcohol at 0.75 and 0.8 V. The last may be occasioned by its intermediate crystallite size and the highest amount of Pt on the surface. Nevertheless, kinetic currents extracted from the polarization curves recorded for $Pt_2CrCo$/CMK-3-500 and $Pt_2CrCo$/CMK-3-700 are intriguing results since the same values are acquired for both materials. In this sense, new experiments are being conducted.

Further characterization of the catalytic activity of the $Pt_2CrCo$/CMK-3 electrocatalysts was made using mass transport corrected Tafel plots (Figure 10), normalized by the ESA, by plotting E vs. $\log(|j\cdot j_L/(j_L-j)|)$, where $j_L$ is the diffusion limiting current. With this end, experiments recorded at 1600 rpm and 0.002 V $s^{-1}$ in absence of alcohol were employed. The experimental data reveal two Tafel slopes at low (80 mV $dec^{-1}$) and high (200-120 mV $dec^{-1}$) overpotential that indicate a change of the mechanism for the ORR in agreement with those results early published for polycrystalline and carbon supported Pt catalysts [43,44]. Interestingly, the value of the Tafel slope at high overpotentials (E < 0.8 V) decreases with the rise of the thermal treatment. Since the fuel cell cathode operates at approximately 0.7 – 0.8 V, the effect of Tafel slope on the activity of a given electrocatalyst at the working potential is of importance. On the other hand, the

deviation of the Tafel slope to higher values may be attributed to different factors, but the oxides species on the catalyst surface appears as the main responsible [37, 39, 44, 45].

## 4. Conclusions

In the present work, the ORR in the absence and presence of methanol on mesoporous carbon (CMK-3) supported $Pt_2CrCo$ electrocatalysts annealed at different temperatures was investigated. The experimental findings can be summarized as follows:

The rise of the temperature of the thermal treatment provokes several changes in the physicochemical properties of the $Pt_2CrCo$/MCK-3 catalysts. Most important ones include the increment of the crystallite size, the formation of an ordered $Pt_3Cr$ alloy phase, the reduction of the Pt-Pt bond distance, the surface segregation of $Cr_2O_3$ species and the diminution of surface Pt sites with (110) orientation that in turn left only surface active sites with (100) and (111) orientations.

All the parameters described above strongly influence the catalytic activity toward the ORR in acidic medium. Indeed, kinetic parameters indicate that $Pt_2CrCo$/CMK-3-500 and $Pt_2CrCo$/CMK-3-700 develop the best performance toward the ORR in absence and presence of methanol, respectively. The corollary is that in order to achieve a good performance for the ORR in the presence of alcohol, the alcohol tolerance is more important than the intrinsic ORR activity of the catalyst.


## Acknowledgments

This research was funded by the Spanish Ministry of Economy and Competitiveness under projects CTQ2011-28913-C02 and ENE2014-52158-C2 (co-funded by FEDER). L.M. Rivera acknowledges the Canary Government (ACIISI) for its PhD scholarship. V.C. kindly thanks for resources and support provided via membership of the UK Catalysis Hub Consortium and funded by EPSRC (grants EP/K014706/1, EP/K014668/1, EP/K014854/1EP/K014714/1 and EP/M013219/1).


## 5. References


[1] Song C, Zhang J. Electrocatalytic Oxygen Reduction Reaction. In: Zhang J. editor. PEM Fuel Cell Electrocatalysts and Catalyst Layers, London: Springer-Verlag; 2008, p. 89-129.

[2] Larminie J, Dicks A. Direct Methanol Fuel Cells. In: Fuel Cell Systems Explain 2 ed, England: John Wiley & Sons Ltd; 2003, p. 141-160.

[3] Pérez G, Pastor E, Zinola C.F. A novel Pt/Cr/Ru/C cathode catalyst for direct methanol fuel cells (DMFC) with simultaneous methanol tolerance and oxygen promotion. Int. J. Hydrog. Energy 2009; 34: 9523–9530.

[4] Bogdanovskayaz VA, Tarasevich MR, Lozovaya OV. Kinetics and mechanism of oxygen electroreduction on PtCoCr/C catalyst containing 20–40 wt % platinum. Russ .J. Electrochem 2011; 47: 846–860.

[5] Huang Q, Yang H, Tang Y, Lu T, Akins D. Carbon-supported Pt-Co alloy nanoparticles for oxygen reduction reaction. Electrochem. Commun 2006; 8: 1220–1224.

[6] Chang H, Joo SH, C Pak C. Synthesis and characterization of mesoporous carbon for fuel cell applications. J. Mater. Chem 2007; 17: 3078–3088.

[7] Lázaro MJ, Calvillo L, Celorrio V, Pardo JI, Perathoner S, Moliner R. In: Sanders IJ, editor. Carbon Black: Production, Properties and Uses, New York:Nova Science Publishers; 2011, p. 41.

[8] Calvillo L, Gangeri M, Perathoner S, Centi G, Moliner R, Lázaro MJ. Effect of the support properties on the preparation and performance of platinum catalysts supported on carbon nanofibers. J.Power Sources 2009; 192:144–150.

[9] Celorrio V, Calvillo L, Martínez-Huerta MV, Moliner R, Lazaro MJ. Study of the Synthesis Conditions of Carbon Nanocoils for Energetic Applications. Energy Fuels 2010, 24: 3361–3365.

[10] Calvillo L, Celorrio V, Moliner R, Garcia AB, Caméan I, Lazaro MJ. Comparative study of Pt catalysts supported on different high conductive carbon materials for methanol and ethanol oxidation. Electrochim. Acta 2013; 102:19–27.

[11] Walcarius A. Mesoporous materials and electrochemistry. Chem. Soc. Rev 2013; 42: 4098-4140.

[12] Ding J, Chan KY, Ren J, Xiao FS. Platinum and platinum–ruthenium nanoparticles supported on ordered mesoporous carbon and their electrocatalytic performance for fuel cell reactions. Electrochim. Acta 2005; 50: 3131-3141.

[13] Choi WC, Woo SI, Jeon MK, Sohn JM, Kim MR, Jeon HJ. Platinum nanoclusters studded in the microporous nanowalls of ordered mesoporous carbon. Adv. Mater 2004; 17: 46-449.

[14] Liu SH, Lu RF, Huang SJ, Lo AY, Chien SH, Liu SB. Controlled synthesis of highly dispersed platinum nanoparticles in ordered mesoporous carbons. Chem. Commun. 2006; 3435-3437.

[15] Mench MM. Introduction to Fuel Cell. In: Fuel Cell Engines, USA: John Wiley & Sons, Inc.; 2008, p.1-25.

[16] Chen S, Ferreira PJ, Sheng W, Yabuuchi N, Allard LF, Shao Horn Y. Enhanced activity for oxygen reduction reaction on "$Pt_3Co$" nanoparticles: direct evidence of percolated and sandwich-segregation structures. J. Am. Chem. Soc. 2008; 130: 13818–13819.

[17] Hernandez Fernandez P, Rojas S, Ocón P, Gomez de la Fuente JL, Terreros P, Peña MA, García Fierro JL. An opening route to the design of cathode materials for fuel cells based on PtCo nanoparticles. Appl. Catal. B-Environ 2007; 77: 19–28.

[18] Baglio V, Urso CD, Sebastian D, Stassi A, Arico AS. PtCo catalyst with modulated surface characteristics for the cathode of direct methanol fuel cells. Int. J. Hydrog. Energy 2014; 39: 5399-5405.

[19] Jeon MK, Zhang Y, McGinn PJ. A comparative study of PtCo, PtCr, and PtCoCr catalysts for oxygen electro-reduction reaction. Electrochim. Acta 2010; 55: 5318–5325.

[20] Dong H, Dong L. Electrocatalytic activity of carbon nanotube-supported Pt–Cr–Co tri-metallic nanoparticles for methanol and ethanol oxidations. J. Inorg. Organomet. Polym. 2011; 21:754–757.

[21] Lopes T, Antolini E, Colmati F, Gonzalez ER. Carbon supported Pt–Co (3:1) alloy as improved cathode electrocatalyst for direct ethanol fuel cells. J. Power Sources 2007; 164: 111–114.

[22] Salgado JRC, Antolini E, Gonzalez ER. Carbon supported Pt–Co alloys as methanol-resistant oxygen-reduction electrocatalysts for direct methanol fuel cells. Appl. Catal. B-Environ 2005; 57: 283–290.

[23] Ryoo R, Hoon S, Kruk, JM, Jaroniec M, Ordered Mesoporous Carbons. Adv. Mater. 2001; 13: 677-681.

[24] Calvillo L, Celorrio V, Moliner R, Cabot PL, Esparbé I, Lázaro MJ. Control of textural properties of ordered mesoporous materials. Microporous and Mesoporous Mater.2008;116:292–298

[25] Lazaro MJ, Calvillo L, Bordeje EG, Moliner R, Ruiz CR. Functionalization of ordered mesoporous carbons synthesized with SBA-15 silica as template. Microporous and Mesoporous Mater. 2007; 103:158–165.

[26] Pires FI, Villullas HM. Pd-based catalysts: Influence of the second metal on their stability and oxygen reduction activity. Int. J. Hydrog. Energy 2012; 37: 7052–17059.

[27] Vogel W J. Interaction of a Nanosized Pd Catalyst with Active C from the Carbon Support: An Advanced in Situ XRD Study. Phys. Chem.C 2011; 115: 1506-1512.

[28] Wagner CD, Riggs WM, Davis LE, Moulder JF, Muilenberg GE.Handbook of x-ray photoelectron spectroscopy. USA: Perkin-Elmer corporation physical electronic division; 1979.

[29] García G, Silva-Chong JA, Guillen-Villafuerte O, Rodríguez JL, Gonzalez ER , Pastor E. CO tolerant catalysts for PEM fuel cells Spectroelectrochemical studies. Catal. Today 2006; 116: 415-421.

[30] Antolini E, Salgado JRC, Santos LGRA, García G, Ticianelli EA, Pastor E, González ER, Carbon supported Pt-Cr alloys as oxygen-reduction catalysts for direct methanol fuel cells. J. Appl. Electrochem. 2006; 36: 355-362.

[31] Kang M, Bae YS, Lee CH, Effect of heat treatment of activated carbon supports on the loading and activity of Pt catalyst. Carbon 2005; 43:1512–1516.

[32] Bezerra CWB, Zhang L, Liu H, Lee K, Marques ALB, Marques EP, et al. A review of heat-treatment effects on activity and stability of PEM fuel cell catalysts for oxygen reduction reaction. J. Power Source 2007;173:891-908.

[33] Rivera Gavidia LM, García G, Anaya D, Querejeta A, Alcaide F, Pastor E. Carbon-supported Pt-free catalysts with high specificity and activity toward the oxygen reduction reaction in acidic medium. Appl. Catal. B-Environ 2016;184:12-19.

[34] Zeid EFA, Hee DK, Lee S, Kim Y. Temperature dependence of morphology and oxygen reduction reaction activity for carbon-supported Pd-Co electrocatalysts J. Appl. Electrochem. 2010;40:1917-1923.

[35] Ma J, Habrioux A, Alonso-Vante N. The Effect of Substrates at Cathodes in Low-temperature Fuel Cells. ChemElectroChem 2014;1:37-46.

[36] Arico AS, Shukl AK, Kim H, Park S, Min M, Antonucci V. An XPS study on oxidation states of Pt and its alloys with Co and Cr and its relevance to electroreduction of oxygen. Appl. Surf. Sci 2001;172:33-40

[37] Ramaswamy N, Mukerjee S. Influence of Inner- and Outer-Sphere Electron Transfer Mechanisms during Electrocatalysis of Oxygen Reduction in Alkaline Media. . Phys. Chem. C 2011;115:18015-18026.

[38] Schmidt J, Gasteiger HA, Stab GD, Urban PM, KoIb DM, Behm RJ. Characterization of High-Surface-Area Electrocatalysts Using a Rotating Disk Electrode Configuration. J. Electrochem Soc 1998;145:2354-2358.

[39] Knani S, Chirchi L, Napporn WT, Baranton S, Léger JM, Ghorbel A. Promising ternary Pt–Co–Sn catalyst for the oxygen reduction reaction. J. Electroanal. Chem 2015;738:145-153.

[40] Cappellari PS, García G, Florez-Montano J, Barbero CA, Pastor E, Planes GA. Enhanced formic acid oxidation on polycrystalline platinum modified by spontaneous deposition of gold. Fourier transform infrared spectroscopy studies. J. Power Source 2015;296:290-297.

[41] Ponce de León C, Low CTJ, Kear AEG, Walsh FC. Strategies for the determination of the convective-diffusion limiting current from steady state linear sweep voltammetry. J. Appl. Electrochem 2007;37:1261-1270.

[42] Anastasijevic NA, Vesovic VB, Adzic RR. Determination of the kinetic parameters of the oxygen reduction reaction using the rotating ring-disk electrode. J. Electroanal. Chem 1987;229: 305-316.

[43] Gasteiger HA, Kocha SS, Sompalli B, Wagner FT. Activity benchmarks and requirements for Pt, Pt-alloy, and non-Pt oxygen reduction catalysts for PEMFCs. Appl. Catal. B-Environ 2005;56:9-35.

[44] Oezaslan M, Strasser P. Activity of dealloyed $PtCo_3$ and $PtCu_3$ nanoparticle electrocatalyst for oxygen reduction reaction in polymer electrolyte membrane fuel cell. J. Power Source 2011;196:5240-5249.

[45] Ge J, St-Pierre J, Zhai Y. PEMFC cathode catalyst contamination evaluation with a RRDE-Acetonitrile. Electrochim Acta 2014;134:272-280.

**Figure caption**

**Figure 1.** X-ray diffraction patterns of $Pt_2CrCo$/CMK-3 electrocatalysts.

**Figure 2.** Crystallite size and Pt-Pt interplanar spacing *versus* temperature of the thermal treatment.

**Figure 3.** Pt 4f (a), Cr 2p (b) and Co 2p (c) core-level spectra of $Pt_2CrCo$/CMK-3 electrocatalysts.

**Figure 4.** Surface atomic ratio and electroactive surface area (ESA) (top panel), and surface species ratio (bottom panel) *versus* temperature of thermal treatment.

**Figure 5.** Blank cyclic voltammetry for $Pt_2CrCo$/CMK-3 electrocatalysts recorded in 0.5 M $H_2SO_4$ at 0.02 V $s^{-1}$. Current density normalized with respect to the ESA.

**Figure 6.** CO stripping voltammograms for $Pt_2CrCo$/CMK-3 electrocatalysts recorded in 0.5 M $H_2SO_4$ at 0.02 V $s^{-1}$. Current density normalized with respect to the ESA.

**Figure 7.** Steady-state polarization curves for $O_2$ reduction at 1600 rpm in 0.5 M $H_2SO_4$ solution at 25 ºC for $Pt_2CrCo$/CMK-3 electrocatalysts. Bottom panel: Current density normalized with respect to the ESA. Scan rate: 0.002 V $s^{-1}$.

**Figure 8**. Steady-state polarization curves for $O_2$ reduction at 1600 rpm in 0.5 M $H_2SO_4$ / 0.5 M $CH_3OH$ (left panels (a)) and 0.5 M $H_2SO_4$ / 3.0 M $CH_3OH$ (right panels (b)) solution at 25 ºC for $Pt_2CrCo$/CMK-3 electrocatalysts. Bottom panels: Current density normalized with respect to the ESA. Scan rate: 0.002 V $s^{-1}$.

**Figure 9.** Koutecky-Levich plots for the ORR in 0.5 M $H_2SO_4$ (methanol free solution) on $Pt_2CrCo$/CMK-3 electrocatalysts.

**Figure 10.** Tafel plots for the ORR in 0.5 M $H_2SO_4$ (methanol free solution) on $Pt_2CrCo$/CMK-3 electrocatalysts. Current density normalized with respect to the ESA.

**Table 1.** Macroscopic and mesoscopic properties of the CMK-3-R8 carbon support.

**Table 2.** Surface composition from XPS and structural characteristics from XRD analysis of $Pt_2CrCo$/CMK-3 electrocatalysts.

**Table 3.** Binding energy (e.V.) and oxidation state distribution (%) from XPS of $Pt_2CrCo$/CMK-3 electrocatalysts.

**Table 4.** ORR kinetic parameters, electroactive surface area (ESA) and EASA (ESA normalized with respect to the loading of Pt) of $Pt_2CrCo$/CMK-3 electrocatalysts.

# Supporting information

## Methanol tolerant $Pt_2CrCo$ catalysts supported on ordered mesoporous carbon for the cathode of DMFC (Code A2_99)

L.M. Rivera Gavidia[1], G. García[1*], V. Celorrio[2, a], M.J Lázaro[2], E. Pastor [1*]

[1]*Instituto de Materiales y Nanotecnología, Universidad de La Laguna, Avda. Astrofísico Francisco Sánchez s/n, 38071 La Laguna, Santa Cruz de Tenerife, Spain*

[2] *Instituto de carboquímica (CSIC) Miguel Luesma Castan 4, 50018 Zaragoza, Spain*

* Corresponding author. Tel.: +34 922 318071; fax: +34 922 318002

E-mail address: ggarcia@ull.edu.es (Gonzalo García).

E-mail address: epastor@ull.edu.es (Elena Pastor).

[a]Present Address: School of Chemistry, University of Bristol, Cantocks Close, Bristol BS8 1TS, United Kingdom

**Description of the TEM and size distribution figures.**

Figures 1SI-6SI display TEM micrographs of the electrocatalysts and size distribution of the metal nanoparticles. They show that $Pt_2CrCo$ is uniformly and highly dispersed on the catalyst support. In agreement with XRD analysis, the thermal treatment slightly increases the average particle size due to some agglomeration or sintering of the metallic nanoparticles.

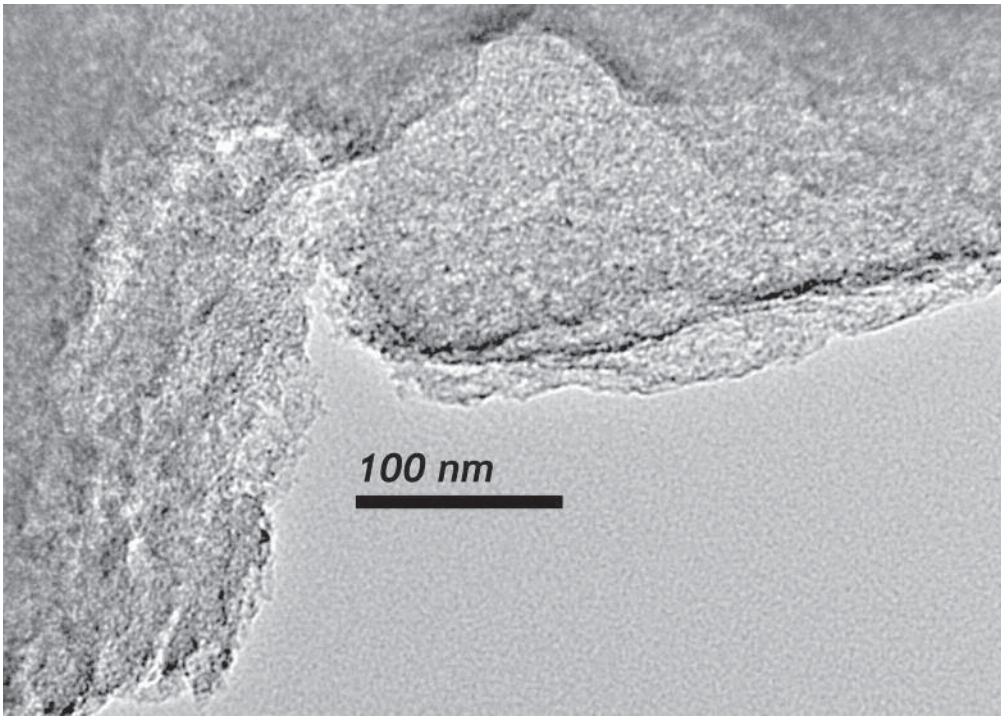


Figure 1SI. TEM image of CMK-3.

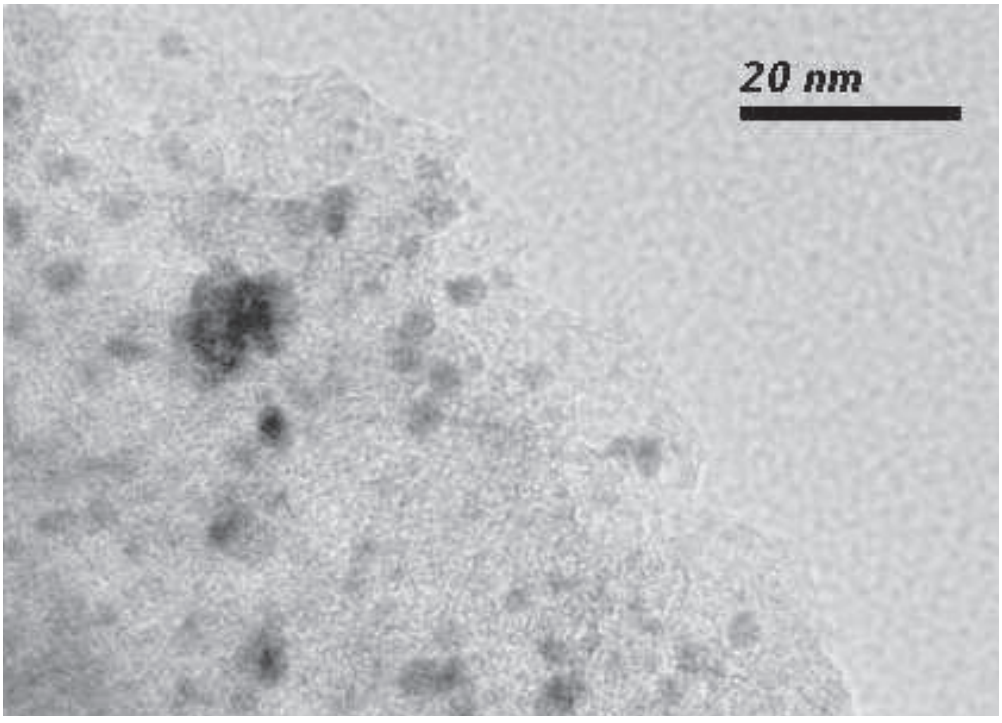


Figure 2SI. TEM image of CMK-3-WTT.

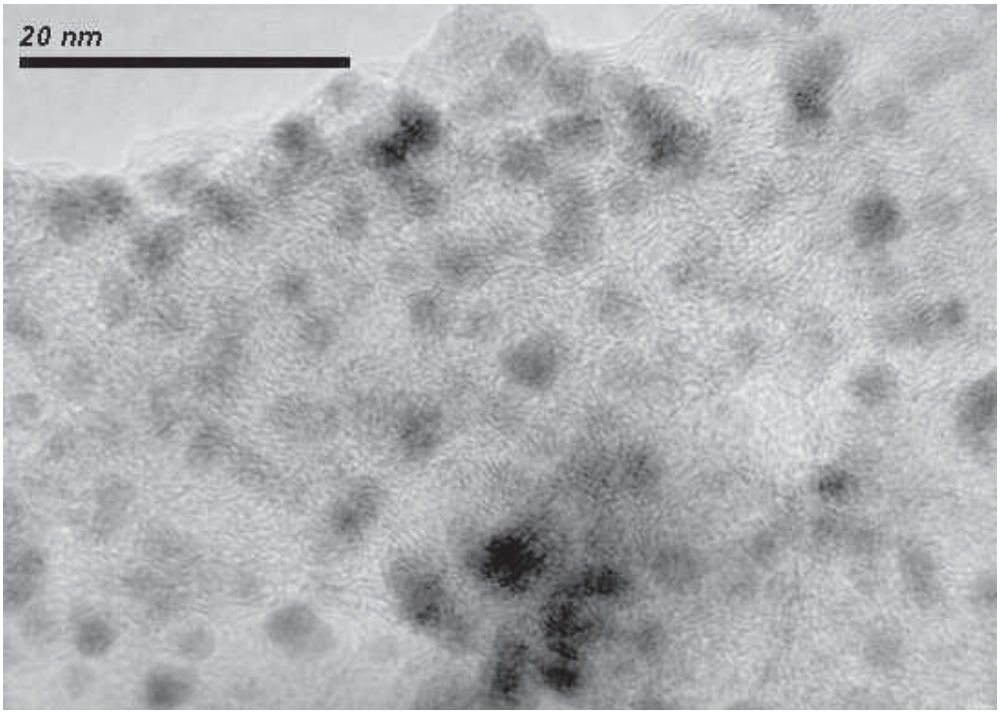


Figure 3SI. TEM image of CMK-3-300.

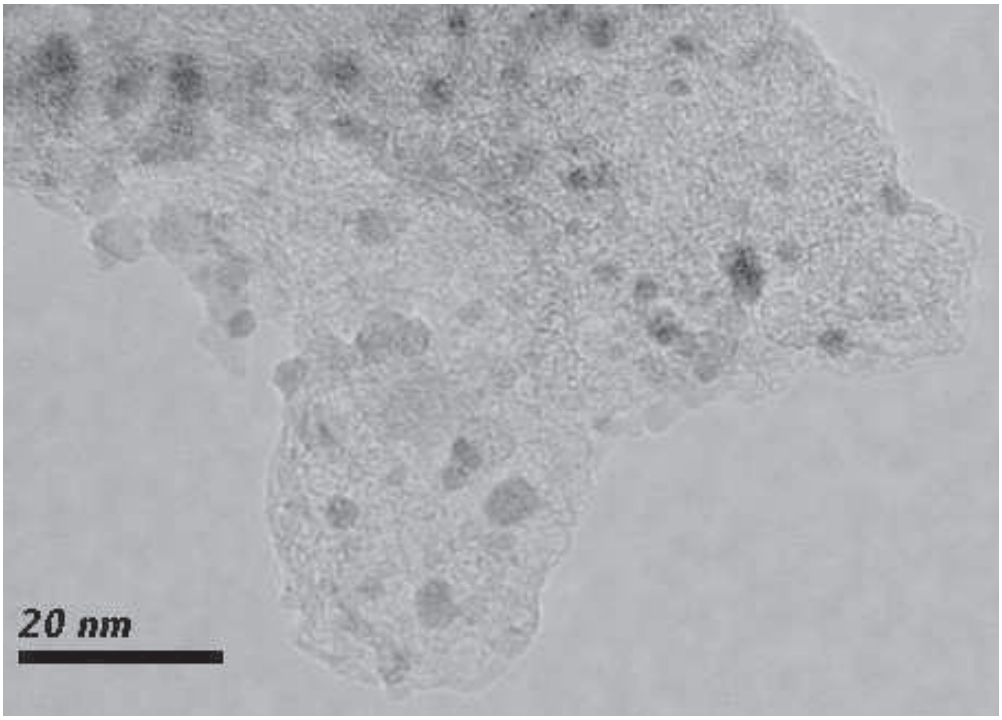


Figure 4SI. TEM image of CMK-3-500.

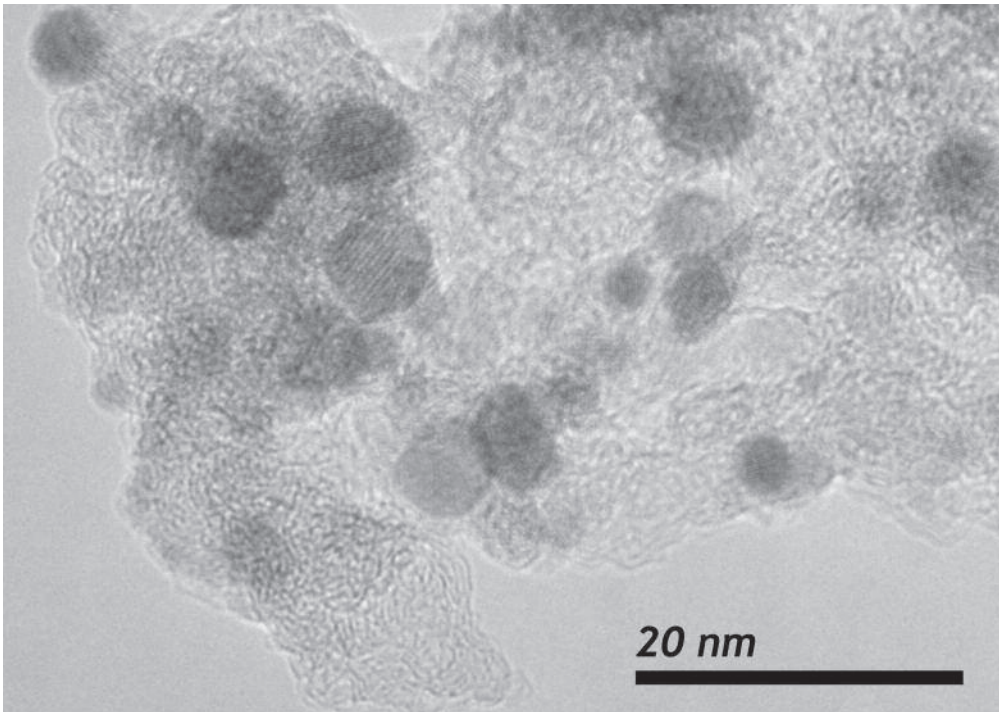


Figure 5SI. TEM image of CMK-3-700.

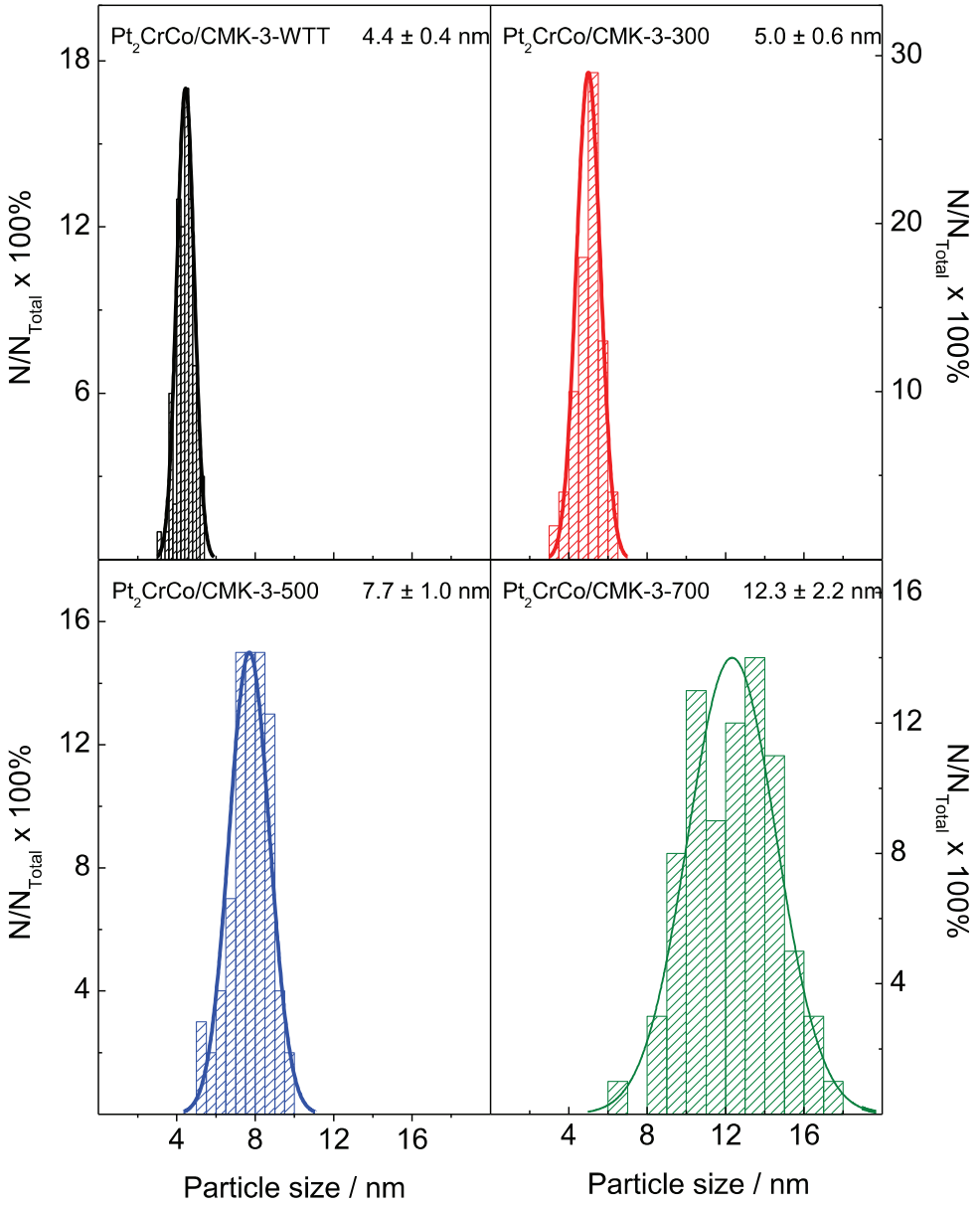


Figure 6SI. Particle size distribution.

Figure 1.

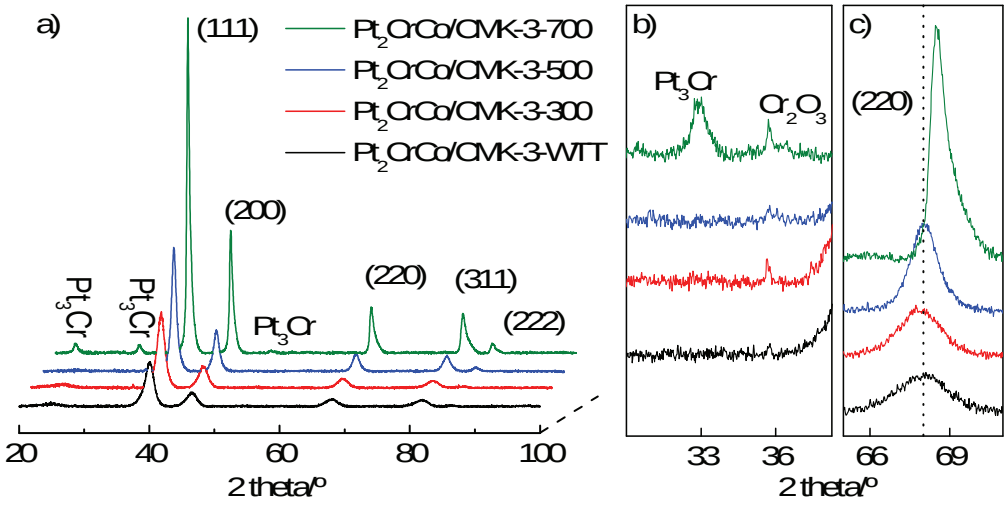
a)
(111)
Pt2CrCo/CMK-3-700
Pt2CrCo/CMK-3-500
Pt2CrCo/CMK-3-300
Pt2CrCo/CMK-3-WIT
(200)
(220)
(311)
(222)
Pt3Cr
Pt3Cr
Pt3Cr
20
40
60
80
100
2 theta/°
b)
Pt3Cr
Cr2O3
33
36
c)
(220)
66
69
2 theta/°

Figure 2.

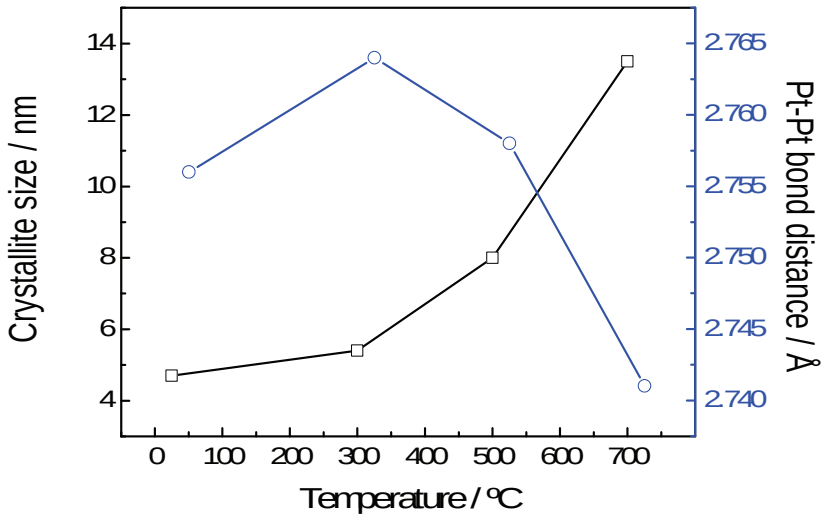
Crystallite size / nm
Pt-Pt bond distance / Å
Temperature / °C
14
12
10
8
6
4
2.765
2.760
2.755
2.750
2.745
2.740
0
100
200
300
400
500
600
700

Figure 3.

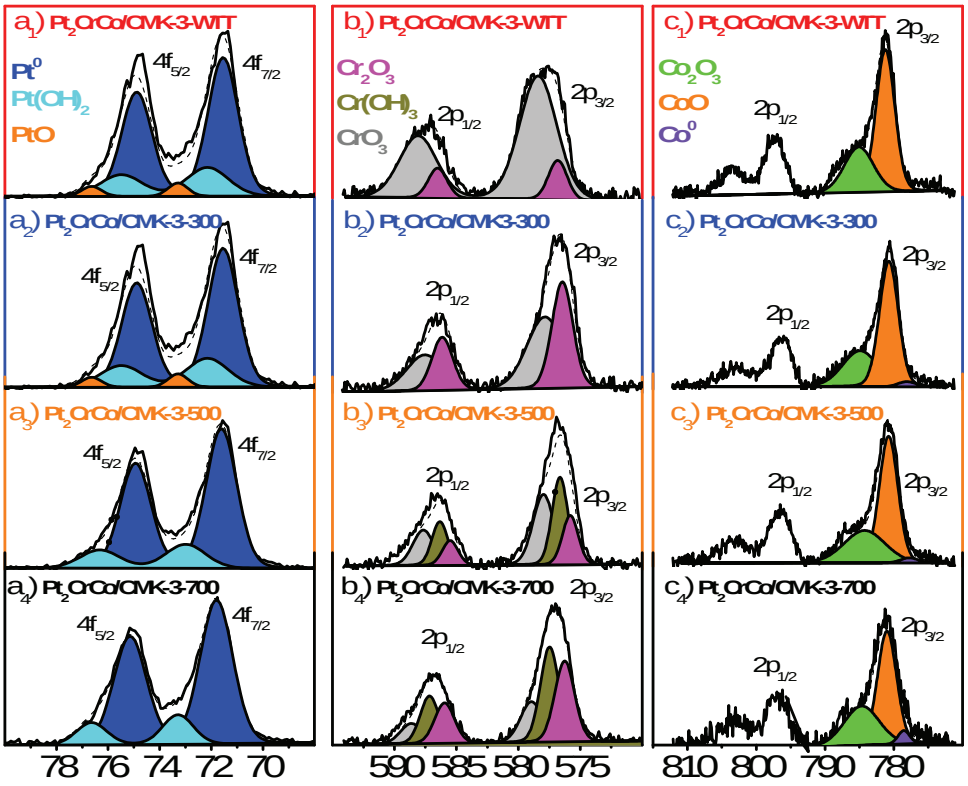
a1) Pt2CrCo/CMK-3-WIT
Pt0
Pt(OH)2
PtO
4f5/2
4f7/2
b1) Pt2CrCo/CMK-3-WIT
Cr2O3
Cr(OH)3
CrO3
2p1/2
2p3/2
c1) Pt2CrCo/CMK-3-WIT
Co2O3
CoO
Co0
2p1/2
2p3/2
a2) Pt2CrCo/CMK-3-300
b2) Pt2CrCo/CMK-3-300
c2) Pt2CrCo/CMK-3-300
a3) Pt2CrCo/CMK-3-500
b3) Pt2CrCo/CMK-3-500
c3) Pt2CrCo/CMK-3-500
a4) Pt2CrCo/CMK-3-700
b4) Pt2CrCo/CMK-3-700
c4) Pt2CrCo/CMK-3-700
78 76 74 72 70
590 585 580 575
810 800 790 780

Figure 4.

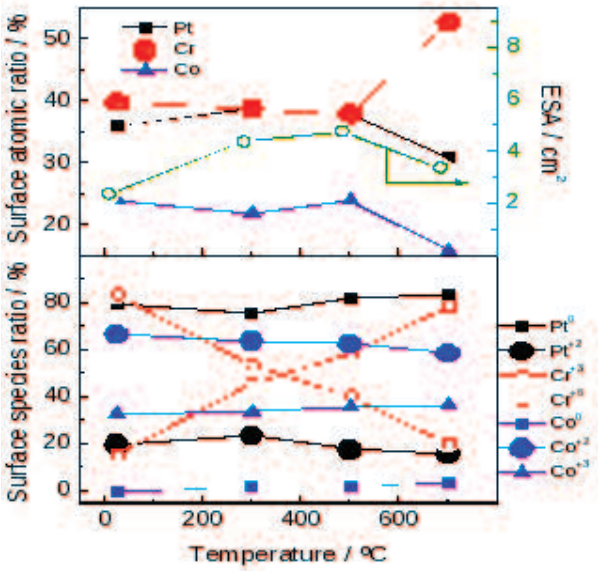
Surface atomic ratio / %
Pt
Cr
Co
ESA / cm²
Surface species ratio / %
Pt⁰
Pt⁺²
Cr⁺³
Cr⁺⁶
Co⁰
Co⁺²
Co⁺³
Temperature / ºC

Figure 5

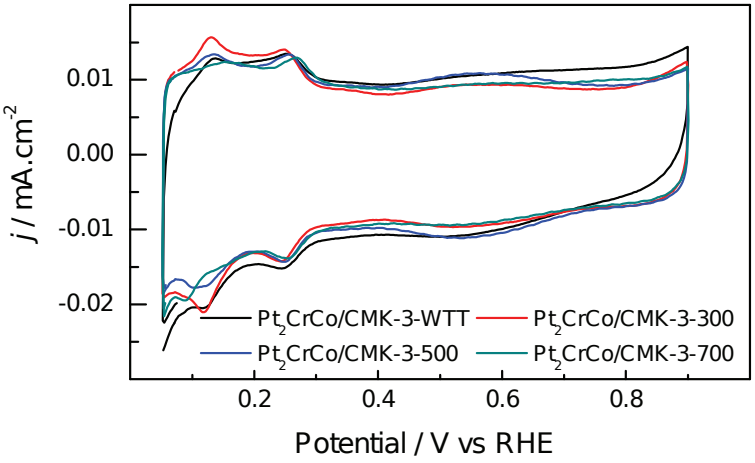
0.01
0.00
-0.01
-0.02
j / mA.cm-2
0.2
0.4
0.6
0.8
Potential / V vs RHE
Pt2CrCo/CMK-3-WTT
Pt2CrCo/CMK-3-300
Pt2CrCo/CMK-3-500
Pt2CrCo/CMK-3-700

Figure 6.

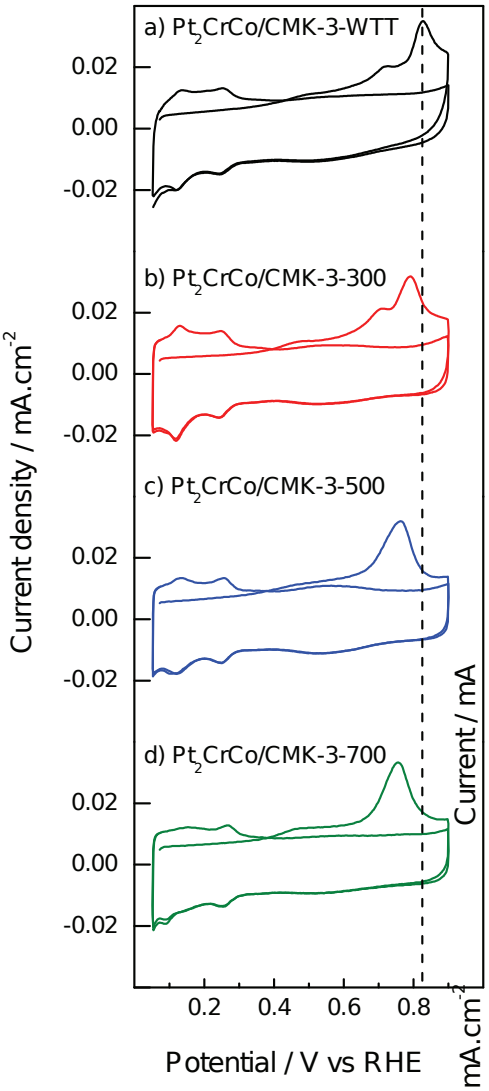


Figure 7.

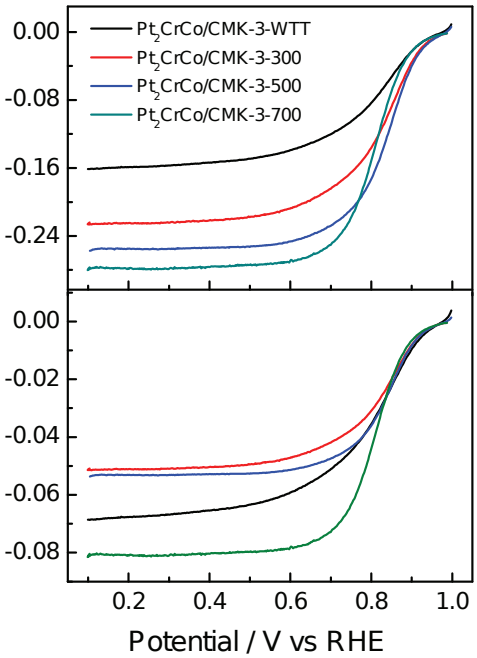

Figure 8.

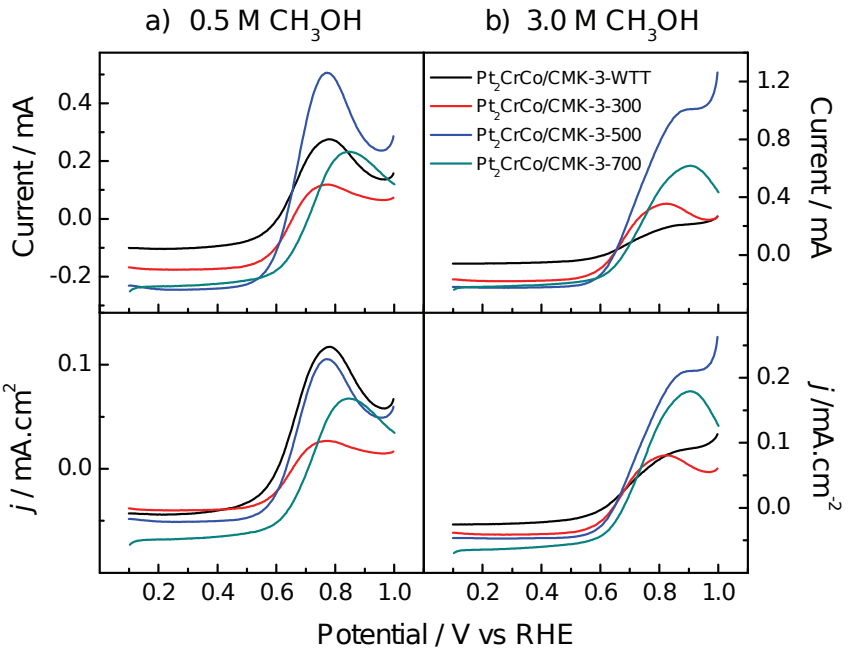
a) 0.5 M CH3OH
b) 3.0 M CH3OH
Pt2CrCo/CMK-3-WTT
Pt2CrCo/CMK-3-300
Pt2CrCo/CMK-3-500
Pt2CrCo/CMK-3-700
Current / mA
j / mA.cm2
j /mA.cm-2
Potential / V vs RHE

Figure 9.

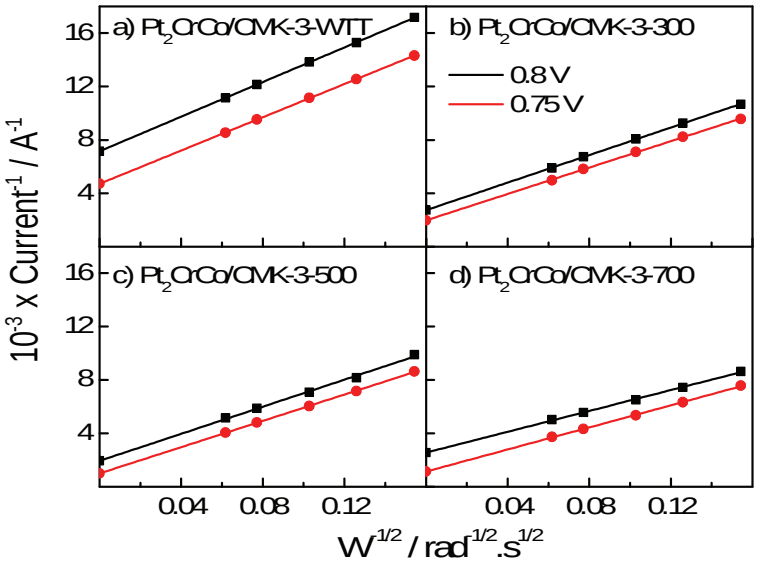
a) Pt2CrCo/CMK-3-WTT
b) Pt2CrCo/CMK-3-300
c) Pt2CrCo/CMK-3-500
d) Pt2CrCo/CMK-3-700
0.8 V
0.75 V
10-3 x Current-1 / A-1
W1/2 / rad-1/2.s1/2
4
8
12
16
0.04
0.08
0.12

Figure 10.

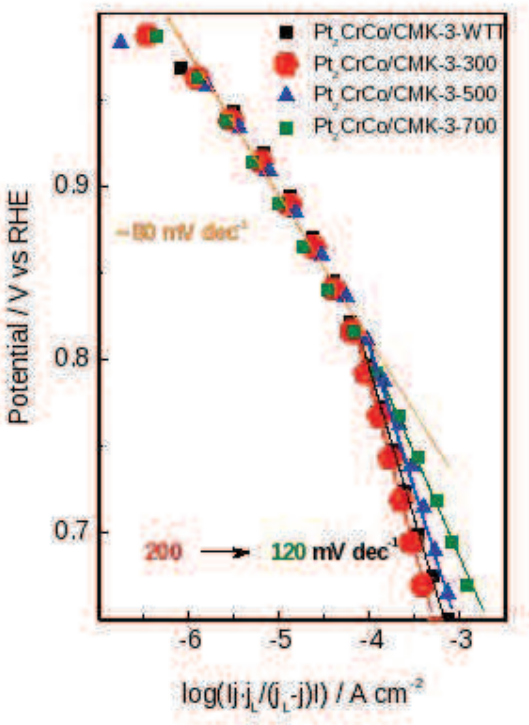
Pt3CrCo/CMK-3-WT
Pt3CrCo/CMK-3-300
Pt3CrCo/CMK-3-500
Pt3CrCo/CMK-3-700
~80 mV dec-1
200
120 mV dec-1
Potential / V vs RHE
0.9
0.8
0.7
-6
-5
-4
-3
log(|j·jL/(jL-j)|) / A cm-2

Table 1

| Sample | $A_{BET}$ $m^2 g^{-1}$ | $V_{total}$ $cm^3 g^{-1}$ | $A_{Meso}$ $m^2 g^{-1}$ | $V_{Meso}$ $cm^3 g^{-1}$ | Pore size (nm) |
|---|---|---|---|---|---|
| CMK-3-R8 | 273 | 0.26 | 238 | 0.24 | 3.5 |

Table ~~1~~2.

| Catalyst | Average crystallite size (nm) | Lattice parameter (Å) | Pt-Pt interplanar spacing (Å) | Surface atomic ratio (XPS) | Bulk atomic ratio (EDX) |
|---|---|---|---|---|---|
| $Pt_2CrCo$/CMK-3-WTT | 4.7 | 3.898 | 2.756 | $Pt_{36}Cr_{40}Co_{24}$ | $Pt_{49}Cr_{27}Co_{24}$ |
| $Pt_2CrCo$/CMK-3-300 | 5.4 | 3.909 | 2.764 | $Pt_{39}Cr_{39}Co_{22}$ | $Pt_{50}Cr_{24}Co_{26}$ |
| $Pt_2CrCo$/CMK-3-500 | 8.0 | 3.901 | 2.758 | $Pt_{38}Cr_{38}Co_{24}$ | $Pt_{49}Cr_{24}Co_{27}$ |
| $Pt_2CrCo$/CMK-3-700 | 13.5 | 3.877 | 2.741 | $Pt_{31}Cr_{53}Co_{16}$ | $Pt_{49}Cr_{26}Co_{25}$ |

Table ~~2~~3.

| Element | Platinum | | Chromium | | Cobalt | | |
|---|---|---|---|---|---|---|---|
| Species | $Pt^0$ | $Pt^{2+}$ | $Cr^{3+}$ | $Cr^{6+}$ | $Co^0$ | $Co^{2+}$ | $Co^{3+}$ |
| Catalysts | | | | | | | |
| $Pt_2CrCo$-WTT | 71.5 (80) | 72.1/73.3 (20) | 576.8 (16) | 578.4 (84) | - | 781.3 (67) | 785.1 (33) |
| $Pt_2CrCo$-300 | 71.3 (76) | 72.2/73.3 (24) | 576.4 (46) | 577.8 (54) | 778.1 (2) | 780.7 (64) | 784.9 (34) |
| $Pt_2CrCo$-500 | 71.6 (82) | 72.9 (18) | 575.8/576.6 (21/38) | 577.9 (41) | 777.7 (2) | 780.7 (63) | 784.3 (36) |
| $Pt_2CrCo$-700 | 71.8 (84) | 73.3 (16) | 576.2/577.5 (37/42) | 578.9 (21) | 778.5 (4) | 781 (59) | 784.7 (37) |

Table ~~3~~4.

| Catalysts | Electron transferred (*n*) | | $j_k^a$ | | $j_k^b$ | EASA ($m^2.gPt^{-1}$) | ESA ($cm^2$) |
|---|---|---|---|---|---|---|---|
| | **0.8 V** | **0.75 V** | **0.8 V** | **0.75 V** | **0.9 V** | | |
| $Pt_2CrCo$-WTT | 2.5 | 2.6 | 2 | 3.1 | 0.14 | 16.8 | 2.4 |
| $Pt_2CrCo$-300 | 3.2 | 3.3 | 5.1 | 7.3 | 0.49 | 31.5 | 4.4 |
| $Pt_2CrCo$-500 | 3.2 | 3.3 | 7.4 | 14.2 | 0.54 | 34.3 | 4.8 |
| $Pt_2CrCo$-700 | 4 | 4 | 5.7 | 12.6 | 0.54 | 24.6 | 3.4 |

*a. From Koutecky-Levich plots ($mA/cm^2$)*
*b. From polarization curves at 1600 rpm and 0.9 V ($mA/cm^2$)*